Polymorphic tandem repeats shape single-cell gene expression across the immune landscape

Hope A. Tanudisastro[1,2,3,4], Anna S.E. Cuomo[1,2,3,5,6], Ben Weisburd[7,8], Matthew Welland[1,2,3], Eleanor Spenceley[3,5,6], Michael Franklin[1,2,3], Angli Xue[3,5,6], Blake Bowen[3,5,6], Kristof Wing[9,10,11], Owen Tang[12,13], Michael Gray[12,13], Andre L.M. Reis[3,14], Jonathan Margoliash[15], Edibe Nehir Kurtas[16,17], Jeffrey Pullin[18], Arthur S. Lee[16,17], Harrison Brand[16,17], Michael Harper[1,2,3], Katalina Bobowik[1,2,3], Michael Silk[1,2,3], John Marshall[1,2,3], Vivian Bakiris[1,2,3], Bindu Swapna Madala[1,2,3], Caitlin Uren[1,2,3], Caitlin Bartie[3,5,6], Anne Senabouth[3,5,6], Harriet Dashnow[19], Liam Fearnley[20,21,22], Egor Dolzhenko[23], Zhen Qiao[3,14], Stuart Grieve[12,13], Tung Nguyen[12,13], Michael Talkowski[16,17], Stephen I. Alexander[4,24], Owen M. Siggs[3,14], Leonhard Gruenschloss[1,2,3], Hannah R. Nicholas[1,2,3], Jennifer Piscionere[1,2,3], Cas Simons[1,2,3], Chris Wallace[18,25], Melissa Gymrek[15,26], Ira W. Deveson[3,14], Alex W. Hewitt[9,10,11], Gemma A. Figtree[12,13], Katrina M. de Lange[1,2,3], Joseph E. Powell[3,5,6,*], Daniel G. MacArthur[1,2,3,*]

[1]Centre for Population Genomics, Garvan Institute of Medical Research, Sydney, NSW, Australia

[2]Centre for Population Genomics, Murdoch Children's Research Institute, Melbourne, VIC, Australia

[3]Faculty of Medicine and Health, University of New South Wales, Sydney, NSW, Australia

[4]Faculty of Medicine and Health, University of Sydney, Sydney, NSW, Australia

[5]Garvan-Weizmann Centre for Cellular Genomics, Garvan Institute of Medical Research, Sydney, NSW, Australia

[6]UNSW Cellular Genomics Futures Institute, University of New South Wales, Sydney, NSW, Australia

[7]Program in Medical and Population Genetics, Broad Institute of MIT and Harvard, Cambridge, MA. USA

[8]Analytic and Translational Genetics Unit, Massachusetts General Hospital, Boston, MA, USA

[9]Menzies Institute for Medical Research, University of Tasmania, Hobart, TAS, Australia

[10]Department of Ophthalmology, Royal Hobart Hospital, Hobart, TAS, Australia

[11]Centre for Eye Research Australia, University of Melbourne, East Melbourne, VIC, Australia

[12]Charles Perkins Centre, The University of Sydney, Sydney, NSW, Australia

[13]Kolling Institute of Medical Research, Royal North Shore Hospital, Sydney, NSW, Australia

[14]Genomics and Inherited Disease Program, Garvan Institute of Medical Research, Sydney, NSW, Australia

[15]Department of Medicine, University of California San Diego, CA, USA

[16]Massachusetts General Hospital, Boston, MA, USA

[17]The Broad Institute of MIT and Harvard, Cambridge, MA, USA

[18]MRC Biostatistics Unit, University of Cambridge, UK

[19]Department of Biomedical Informatics, University of Colorado Anschutz Medical Campus, Aurora, CO, USA

[20]Population Health and Immunity Division, The Walter and Eliza Hall Institute of Medical Research, Parkville, VIC 3052, Australia

[21]Department of Medical Biology, University of Melbourne, Parkville, VIC, Australia

[22]Bruce Lefroy Centre, Murdoch Children's Research Institute, Parkville, VIC, Australia

[23]Pacific Biosciences of California, Menlo Park, CA, USA

[24]Centre for Kidney Research, Kids Research Institute and the Department of Nephrology, The Children's Hospital at Westmead, Westmead, NSW, Australia

[25]Cambridge Institute of Therapeutic Immunology & Infectious Disease, University of Cambridge, UK

[26]Department of Computer Science and Engineering, University of California San Diego

* co-senior

Abstract

Tandem repeats (TRs) - highly polymorphic, repetitive sequences dispersed across the human genome - are crucial regulators of gene expression and diverse biological processes. Yet, due to historical challenges in their accurate calling and analysis, TRs have remained underexplored compared to single nucleotide variants (SNVs). Here, we introduce a cell type-specific resource exploring the impact of TR variation on human gene expression. Leveraging whole genome and single-cell RNA sequencing, we catalog over 1.7 million polymorphic TR loci and their associations with gene expression across more than 5 million blood-derived cells from 1,790 individuals. We identify over 58,000 single-cell expression quantitative trait TR loci (sc-eTRs), 16.6% of which are specific to one of 28 distinct immune cell types. Further fine-mapping uncovers 6,210 sc-eTRs as candidate causal drivers of gene expression in 21% of genes tested genome-wide. We show through colocalization that TRs are likely regulators of over 2,000 GWAS loci associated with immune-mediated and hematological traits, and further identify novel TRs warranting investigation in rare disease cohorts. TRs are pivotal, yet long-overlooked, contributors to cell type-specific gene expression, with promising implications for understanding rare disease pathogenesis and the genetic architecture of complex traits.

Introduction

Advances in sequencing and genotyping tools have extended our understanding of the human genome, allowing for more detailed characterization of classes of genetic variation that were previously challenging to genotype. Among these, tandem repeats (TRs) - highly polymorphic repetitive sequences characterized by 1-6 bp motifs (short tandem repeats [STRs]) and >6bp motifs (variable number tandem repeats [VNTRs]) - have emerged as a key component of genetic diversity with profound biological effects.

More than 2 million polymorphic TR loci comprise 3-5% of the human genome, collectively occupying more genomic real estate than protein coding genes[1,2]. Individual TRs are estimated to be up to 10^4 times more mutable than individual single nucleotide variants (SNVs)[3], making them a rich source of genetic variation. TRs can influence gene expression by regulating transcription factor binding[1], altering nucleosome occupancy[4], and modulating the activity of promoters[5] and enhancers[6]. Despite their clear functional importance, TRs have largely been understudied in population genetics, primarily due to high error rates associated with sequencing and aligning repetitive regions that have historically limited the accuracy of TR genotyping[7]. However, methodological improvements[7] have begun to address these challenges, enabling more precise and comprehensive characterization of TRs.

Rare repeat expansions have been known for several decades[8] to cause severe Mendelian disorders, such as Huntington's disease and Fragile X Syndrome, but emerging evidence suggests that common TR variation is an underexplored source of genetic variation that may help account for the heritability of complex traits. Recent studies have uncovered associations between common TR variation and a diverse array of phenotypes, including gene expression[9], epigenetic modification[10], serum biomarker levels[11], cancer susceptibility[12,13], and other complex disease traits[14]. However, the lack of harmonization in locus definitions[2] across studies presents a significant challenge, making it difficult to

compare results and draw conclusions about the functional impact of TR variation. Some studies[11,15] have also relied on imputation to infer TR genotypes from SNV genotypes which, while useful, is not as reliable as direct genotyping, particularly given that highly polymorphic loci such as TRs are less likely to be in strong linkage disequilibrium with neighboring SNVs.

Expression quantitative trait loci (eQTL) studies play a crucial role in understanding how genetic variation influences biological processes by identifying genetic drivers of variation in gene expression. While studies of how TRs regulate gene expression have primarily relied on bulk tissue data[2,9], recent advances in single-cell RNA sequencing (scRNA-seq)[16] enable the study of cell type-specific effects of TRs at a finer resolution at population scale. Single-cell analysis provides insight into cellular heterogeneity[17], differentiation pathways[18], and disease progression[19]. Long-read scRNA-seq of striatal projection neurons was instrumental in uncovering the key role that somatic TR expansions play in the progression of Huntington's disease[20], subsequently opening new avenues for gene therapy. Integrating TRs in single-cell analyses promises deeper insights into the mechanisms of known TR-associated phenotypes, and may reveal novel functions of these repetitive sequences.

We present a catalog of single-cell expression quantitative trait TR loci (sc-eTRs) from peripheral blood samples in Phase 1 of TenK10K, the largest paired human whole genome and single-cell RNA sequencing dataset to date. We identify more than 58,000 TRs robustly associated with variation in gene expression in at least one cell type, and characterize their cell type specificity, evidence for causality, and potential colocalization with signals previously shown to be associated with a variety of immune and hematological traits.

Results

Genome-wide polymorphic TR discovery

To investigate the relationship between TR length variation and gene expression across 28 immune cell types, we first identified polymorphic TR loci in 1,790 individuals from Phase 1 of the TenK10K initiative for whom both high-coverage whole genome sequencing (WGS) and single-cell RNA sequencing (scRNA-seq) data from over 5 million peripheral blood mononuclear cells (PBMCs) were available (Fig. 1a). Phase 1 of TenK10K consists of the Tasmanian Ophthalmic Biobank cohort (964 European ancestry individuals with no signs of ocular disease) and the BioHEART cohort (826 European ancestry individuals with diagnosed or suspected cardiac disorders) (Methods).

Most TR genotyping tools require target loci to be specified *a priori*, meaning that catalog curation is crucial for sensitivity. To generate a genome-wide catalog of candidate TRs, we merged several reference-based (hg38)[21–24] and cohort-driven polymorphic TR catalogs, using samples from the 1000 Genomes Project[25] and the Human Pangenome Reference Consortium[26], generating a final catalog of 4,918,794 loci[27] (Methods).

To curate a set of loci likely to be sufficiently polymorphic to drive an association signal, we then used ExpansionHunter to genotype these loci in approximately 10% of the cohort, identifying 2,638,529 polymorphic loci for downstream analysis. Homopolymer and dinucleotide motifs comprised the majority of the polymorphic loci, consistent with other polymorphic catalogs[26,28] (Fig. 1b). Polymorphism, measured as per-locus observed

heterozygosity, was lowest in tri- and hexanucleotide motifs, consistent with these motifs having lower reported mutation rates[29] (Fig. 1c). Based on Matched Annotation from NCBI and EBI (MANE)[30], most polymorphic loci were located in intergenic (60.4%) and intronic (37.4%) regions, with others found in promoter (0.7%), coding sequence [CDS] (0.4%) 3' untranslated region [UTR] (0.9%), and 5' UTR (0.2%) regions (Fig. 1d).

Because TR genotyping is prone to stutter and remapping errors, we benchmarked the accuracy of three short-read TR genotyping tools - ExpansionHunter[31,32], HipSTR[23], and GangSTR[22] - by comparing their WGS-derived genotypes with gold standard capillary electrophoresis-derived genotypes of 388 STR loci in 120 samples from the Simons Genome Diversity Project[33] (Fig. S1, Methods). ExpansionHunter had the best performance with a validation rate of 95.0%, followed by HipSTR and GangSTR (94.9%, 87.4% respectively). The performance of ExpansionHunter and HipSTR are comparable to prior validation studies[23,32].

We used ExpansionHunter to genotype TRs in the rest of the cohort, and found that 97.3% of raw genotyped alleles were within 10 repeats of the modal allele of each locus, consistent with the stepwise mutation model[34] (Fig. 1e).

We subsequently filtered for high quality calls and loci for downstream analysis (Methods). Using approximately 1.7 million filtered loci, we further validated the accuracy of ExpansionHunter with PacBio HiFi long-read TR genotypes (n=25 individuals), reporting a strict concordance rate of 79.8%, which increased to 85.6% when allowing for +/- 1 repeat unit difference (Fig. 1f, Methods). As expected, validation rate tended to decrease as TR reference length increased (Fig. 1g). Notably, this PacBio genome-wide approach included TRs in low complexity regions in contrast to the capillary electrophoresis validation dataset described above where TR loci were flanked by non-repetitive sequences and thus had improved read mappability (Note S1).

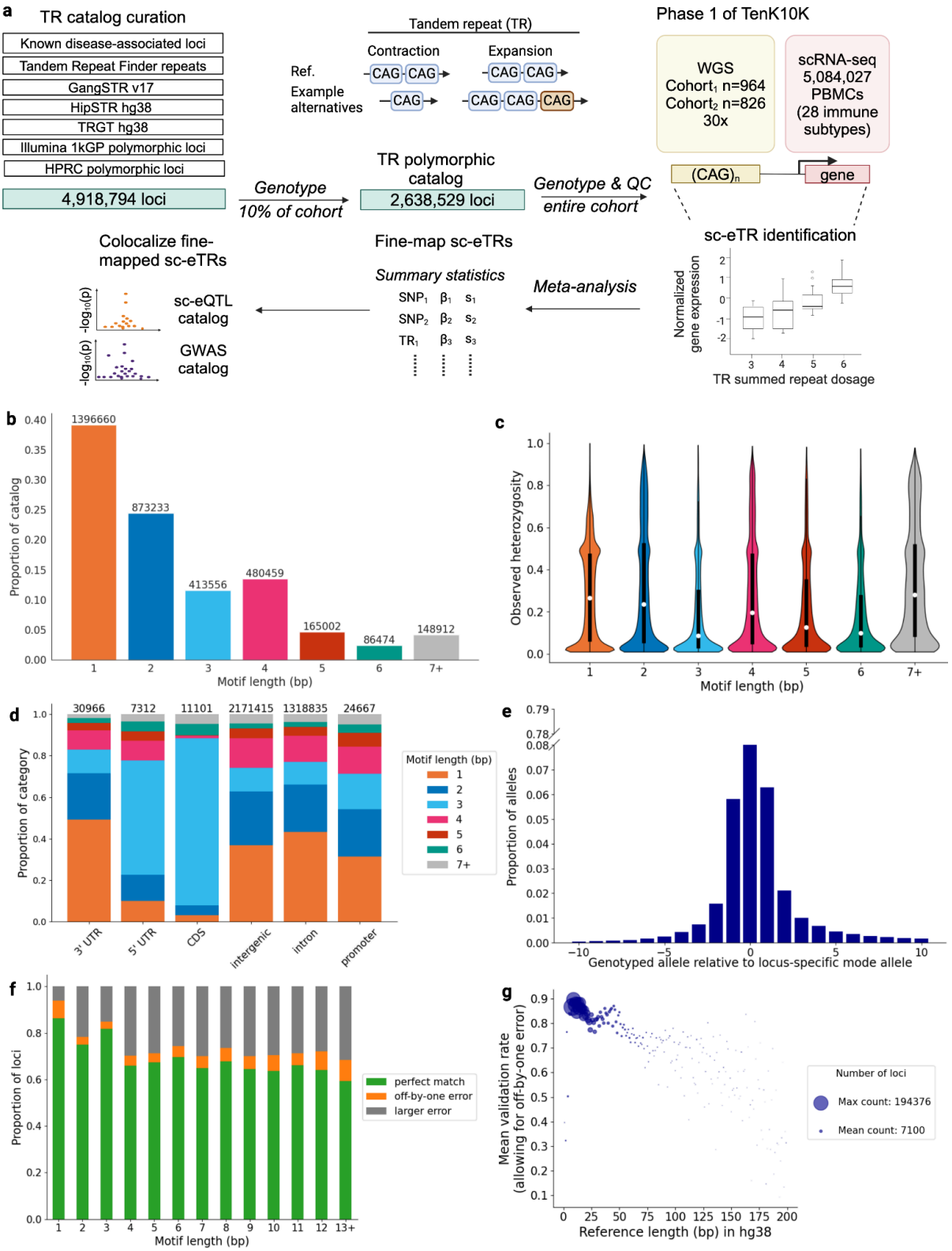
a
TR catalog curation
Known disease-associated loci
Tandem Repeat Finder repeats
GangSTR v17
HipSTR hg38
TRGT hg38
Illumina 1kGP polymorphic loci
HPRC polymorphic loci
4,918,794 loci
Genotype
10% of cohort
TR polymorphic catalog
2,638,529 loci
Genotype & QC
entire cohort
Tandem repeat (TR)
Contraction
Expansion
Ref.
Example alternatives
CAG
Phase 1 of TenK10K
WGS
Cohort1 n=964
Cohort2 n=826
30x
scRNA-seq
5,084,027 PBMCs
(28 immune subtypes)
(CAG)n
gene
sc-eTR identification
Normalized gene expression
TR summed repeat dosage
Meta-analysis
Fine-map sc-eTRs
Summary statistics
SNP1 β1 s1
SNP2 β2 s2
TR1 β3 s3
Colocalize fine-mapped sc-eTRs
-log10(p)
sc-eQTL catalog
GWAS catalog
b
Proportion of catalog
1396660
873233
413556
480459
165002
86474
148912
Motif length (bp)
c
Observed heterozygosity
Motif length (bp)
d
Proportion of category
30966
7312
11101
2171415
1318835
24667
3' UTR
5' UTR
CDS
intergenic
intron
promoter
Motif length (bp)
1
2
3
4
5
6
7+
e
Proportion of alleles
Genotyped allele relative to locus-specific mode allele
f
Proportion of loci
perfect match
off-by-one error
larger error
Motif length (bp)
g
Mean validation rate (allowing for off-by-one error)
Reference length (bp) in hg38
Number of loci
Max count: 194376
Mean count: 7100

Figure 1: Genome-wide polymorphic TR curation and validation. a, Schematic of study design involving TR catalog curation, sc-eTR identification, fine-mapping, and colocalization analysis. **b**, Motif length distribution of TR loci in the polymorphic catalog. **c**, Observed heterozygosity of TR loci in the polymorphic catalog, by motif length. Violin plots summarize the distribution of locus-specific observed heterozygosity rates, showing median values and boxes spanning from the 25th (Q1) to the 75th percentile (Q3). Whiskers extend to Q1 - 1.5 x IQR and Q3 + 1.5 x IQR, where IQR is the interquartile range. **d**, Gene annotation (MANE) of TR loci in the polymorphic catalog, by motif length. **e**, Distribution of genotyped alleles relative to the locus-specific modal allele, restricted to genotyped alleles within 10 repeats of the mode allele. **f**, Validation of ExpansionHunter genotypes using TRGT genotypes derived from PacBio HiFi long read samples (n=25) across 1,777,403 TR loci used in downstream sc-eTR discovery, by motif length. Perfect match calls were those where the ExpansionHunter summed repeat dosage exactly matched that of TRGT, off-by-one error were those where the ExpansionHunter summed repeat dosage was +/- 1 repeat from that of TRGT, with the remaining discordant calls labeled as 'larger error'. **g**, Mean validation rate (allowing for off-by-one error) of ExpansionHunter genotypes using TRGT genotypes (n=25 samples), by reference length (bp) of the TR locus. Horizontal axis is truncated to 200 bp, capturing more than 99.9% of the loci.

Characterization of single-cell expression TRs (sc-eTRs) across 28 immune cell types

We identified *cis* sc-eTRs (*i.e.* eQTL associations with TR variants close to the gene of interest) by testing associations between 1,777,403 common autosomal TRs (non-major allele frequency ≥ 0.5%) and the expression of 21,407 genes across 28 immune cell types. We defined an sc-eTR as an eTR/eGene pair association detected in a given cell type. Using associaTR, we performed pseudobulk eQTL mapping within 100 kb of each gene's transcription start and end sites, controlling for technical and biological covariates (Fig. 1a, Methods). We conducted parallel analyses for common single nucleotide variants (SNVs) (minor allele frequency ≥ 1%) and employed a two-batch meta-analysis approach to mitigate cohort-specific sequencing effects (Fig. S3, Methods).

We identified 58,603 unique sc-eTRs associating with 14,325 eGenes at a gene-level false discovery rate (FDR) of 5% (Fig. 2a, Fig. S4, Table S1). Type 1 error (false positive rate) was controlled, assessed by permutation (Fig. 2a, Methods). The number of sc-eTRs detected in each cell type correlated with the number of cells sequenced in each cell type (Pearson r = 0.93, $P = 6.3\times10^{-13}$), but we detected sc-eTRs in every cell type (Fig. 2a).

After accounting for global effect size sharing and power differences between cell types using multivariate adaptive shrinkage[35], pairwise similarity of cell types was quantified by the correlation of the posterior effect sizes of sc-eTRs, showing patterns of cell type similarity consistent with hierarchical classification, albeit weaker for rarer cell types (Fig. 2b). sc-eTRs were enriched in ENCODE candidate *cis* regulatory elements (cCREs) (odds ratio [OR] = 5.2, Fisher's exact test, $P < 2.2\times10^{-16}$). Among cCRE-overlapping sc-eTRs, the majority were found in distal enhancer-like signatures (Fig. 2c). Considering genomic context, sc-eTRs were enriched in proximal regulatory regions and depleted in coding and intergenic regions (Fig. 2d). Across all sc-eTRs, increasing repeat length generally corresponded to higher gene expression (median effect size = 0.018, Wilcoxon signed-rank test, $P = 5.79\times10^{-5}$). This positive association was most pronounced in sc-eTRs overlapping 5' UTRs and regions with promoter-like signatures ($P = 2.50\times10^{-6}$ and 9.18×10^{-7} respectively, Fig. 2e). Broader effect size distributions were observed in intergenic sc-eTRs compared to those in proximal

regulatory elements (Levene's test, $P = 2.9\times10^{-5}$, Fig. 2e).

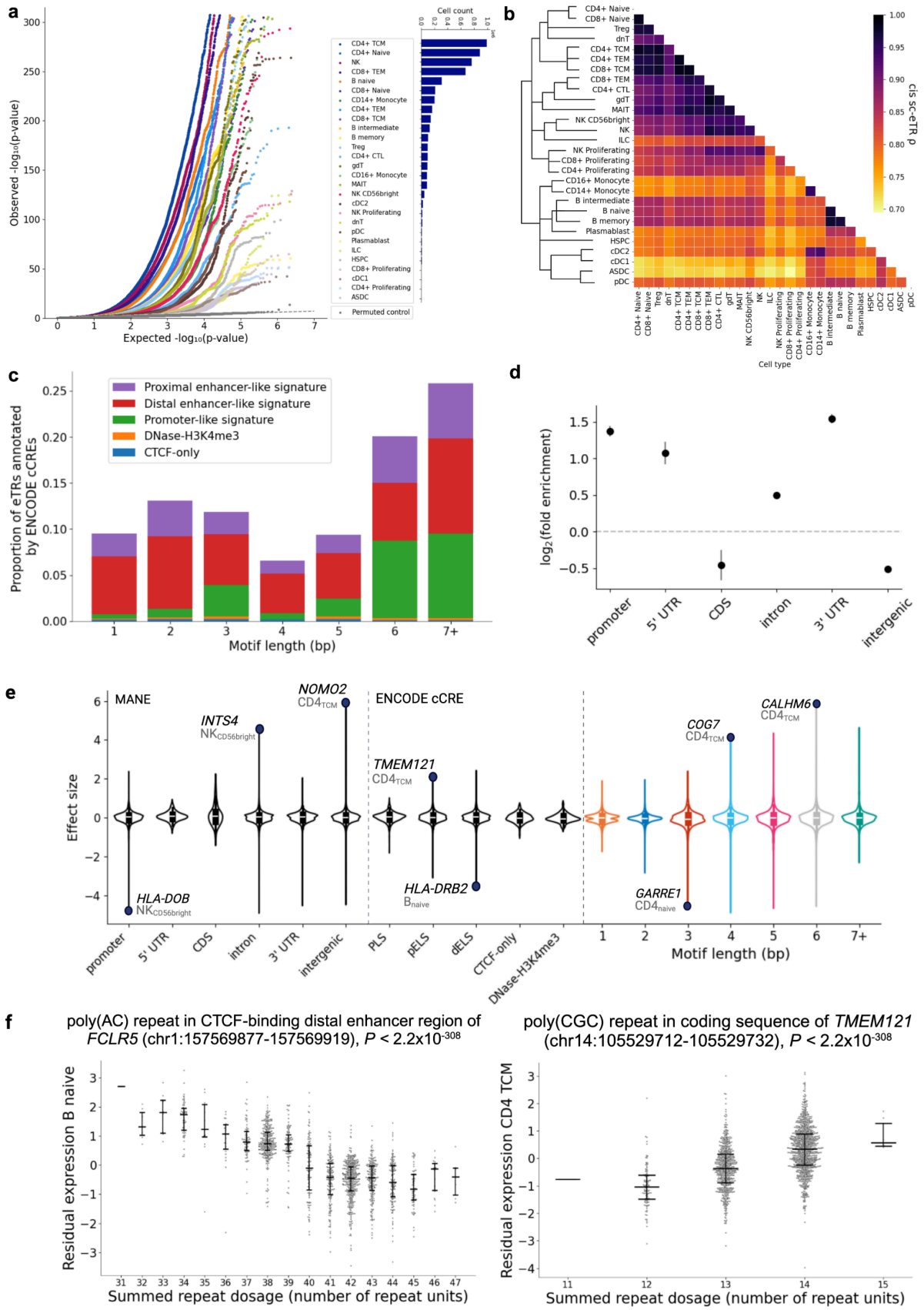

Figure 2: single-cell eTR discovery. a, Quantile-quantile (QQ) plot comparing observed *P* values for each TR x gene test (colored by cell type) against the expected uniform distribution for each cell type (dashed gray line). Permuted control is highlighted in dark gray (n=1,790). **b**, Heatmap of pairwise

correlations of *cis* sc-eTR posterior effect sizes across cell types, adjusted for global effect size sharing and power differences with multivariate adaptive shrinkage[35]. Order of rows and columns reflect scRNA-seq cell type classification by scPred[36] (Methods). **c**, ENCODE candidate *cis* regulatory element (cCRE) annotation of sc-eTRs, by motif length. **d**, Log_2(fold enrichment) of sc-eTRs relative to all TRs genotyped, by MANE gene annotation. Error bars correspond to 95% confidence intervals. **e**, Distributions of effect sizes, by gene annotation (MANE), ENCODE cCRE, and motif length. Violin plots summarize the distribution of effect sizes with horizontal lines showing median values and boxes spanning from the 25th (Q1) to the 75th percentile (Q3). Whiskers extend to Q1 - 1.5 x IQR and Q3 + 1.5 x IQR, where IQR is the interquartile range. Select eGenes and corresponding cell type with outlier effect sizes are labeled. **f**, Examples of single-cell eTRs validated using GTEx whole blood bulk RNA-seq data[9]: a naive B cell-specific poly(AC) repeat associating with expression of *FCRL5*, which encodes an immunoglobulin receptor promoting B cell proliferation[37]; a $CD4_{TCM}$-specific poly(CGC) coding repeat associating with expression of *TMEM121.*

To determine cell type specificity of sc-eTRs, we performed pairwise meta-analyses comparing the effect sizes of sc-eTRs in each cell type against all other cell types where the respective gene was expressed in at least 1% of cells. sc-eTRs were considered shared if the meta-analysis p-value was lower than the original p-value. Conversely, sc-eTRs were considered cell type-specific if the meta-analysis p-value was consistently higher than the original p-value across all pairwise comparisons (Methods).

Of the 58,603 unique sc-eTRs identified, 16.6% were specific to one cell type (*i.e.* cell type-specific). Across all cell types, the median pairwise sharing of top sc-eTRs was 12.4% (minimum = 5.9%, maximum = 55.3%), suggesting the presence of cell type-specific regulatory mechanisms. Monocytes had the highest level of intra-subset sharing (median = 41.1%) while sharing within the CD8+ (median = 35.6%), NK (median = 34.2%), CD4+ (median = 27.4%), and B (median = 24.8%) cell subsets were lower. We tested for enrichment of eGenes associated with cell type-specific sc-eTRs among Gene Ontology (GO)[38–40] terms and recapitulated known functional associations between cell types and their eGenes (Note S2).

Cell type-specific sc-eTRs had greater absolute effect sizes and were, on average, located further away from the transcription start site than shared sc-eTRs (Mann-Whitney U test, $P = 5.58\times10^{-224}$ and $P = 4.07\times10^{-40}$ respectively), consistent with previous observations in cell type-specific eSNVs[41]. Compared to shared sc-eTRs, cell type-specific sc-eTRs were also enriched in distal enhancer-like signatures and depleted in promoter regions, aligning with earlier findings in cell type-specific eSNVs[42] (Fig. S5).

We identified 262 sc-eTRs with opposite signed effect sizes in at least two cell types, highlighting the importance of cell type context in gene expression. A striking example of cell type-specific regulation emerged from a poly(GAAG) intronic repeat overlapping an enhancer of *B4GALT1*. Increasing repeat length was associated with contrasting effects on *B4GALT1* expression (Fig. S6), markedly increasing expression in naive B cells (effect size = 2.23, $P = 4.56\times10^{-66}$) while reducing it in $CD8_{TEM}$ cells (effect size = -1.58, $P = 1.21\times10^{-60}$). Notably, B4GALT1 enhances serum IgG galactosylation in B cells[43], whereas its inhibition augments CD8+ T-cell infiltration via PD-L1 modulation[44]. Thus, repeat length variation in this locus may fine-tune immune responses through cell type-dependent *B4GALT1* expression.

We further considered eTRs previously identified in whole blood bulk RNA-seq GTEx data[9,45] (n = 652 individuals), and found that 91% of them overlapped with nominally significant sc-eTRs ($P < 0.05$) in at least one cell type in our dataset (Fig. 2f, Fig. S4, Table S2, Methods). Signals unique to sc-eTRs were enriched for cell type specificity compared to those overlapping bulk eTRs identified in GTEx (OR = 1.40, Fisher's exact test, $P = 0.0009$).

Functional enrichment and LD profiles of candidate causal sc-eTRs

Despite TRs exhibiting on average higher genotyping uncertainty than SNVs, we identified 9,712 genes where sc-eTRs were the lead variant (*i.e.* exhibited the strongest association signal within their respective *cis* windows compared to the signals of neighboring sc-eTRs and sc-eSNVs). The presence of these lead sc-eTRs suggests either large effect sizes that overcome genotyping uncertainty, or a subset of TR loci with lower genotyping uncertainty. In either case, these lead sc-eTRs are strong candidates for causal drivers of gene expression variation.

From an initial set of 58,603 unique sc-eTRs, we identified 6,210 as candidate causal drivers of gene expression variation (Table S3). In each cell type, candidate causal sc-eTRs were conservatively defined as lead sc-eTRs fine-mapped with a posterior inclusion probability (PIP) ≥ 0.7. To fine-map lead sc-eTRs, we initially attempted SuSiE with 10 maximum credible sets, but identified instability in the results related to meta-analysis and imperfect representation of LD between multiallelic TRs and biallelic SNVs (Note S3). Consequently, we performed fine-mapping with SuSiE by conservatively assuming that each locus has at most one causal variant. Candidate causal sc-eTRs were identified across 4,598 eGenes, suggesting that sc-eTRs were the candidate causal signal in 21% of genes tested in at least one cell type.

Candidate causal sc-eTRs were most enriched in proximal regulatory elements including 5' UTRs, cCREs with promoter-like signatures, and promoter regions (OR = 6.0, 5.0, 3.5 respectively, Fisher's exact test, $P < 2.2\times10^{-16}$ for all comparisons, Fig. 3a). These enrichments were stronger in candidate causal sc-eTRs compared to all sc-eTRs (Fig. S7). Conversely, candidate causal sc-eTRs were negatively enriched in more distal regulatory elements found in intergenic regions (OR = 0.46, Fisher's exact test, $P < 2.2\times10^{-16}$, Fig. 3a). We also observed that GC-rich TRs, defined as loci where guanine and cytosine nucleotides constitute at least 80% of the motif, were enriched in candidate causal sc-eTRs compared to all genotyped TRs (OR = 1.47, Fisher's exact test, $P = 1.35\text{x}10^{-7}$).

Candidate causal sc-eTRs exhibited an inverse relationship with protein-coding constraint, quantified using the loss-of-function observed/expected upper bound fraction (LOEUF) score (Spearman's $\rho = 0.98$, $P = 1.47\times10^{-6}$, Fig. S8); genes under strong evolutionary constraint (low LOEUF deciles) harbored significantly fewer candidate causal sc-eTRs compared to less constrained genes. This finding aligns with the expectation that dosage-sensitive genes - typically characterized by highly constrained coding sequences - face stronger selective pressure against expression-modifying variants, resulting in depletion of regulatory variation[46].

We then considered enrichment of candidate causal sc-eTRs in non-coding regulatory constraint elements across species. By leveraging both Zoonomia[47] and primate-specific[48]

annotations, we found that these sc-eTRs exhibited preferential enrichment for transcription factor binding sites (TFBS) within constrained primate-specific non-coding elements while showing attenuated enrichment in more deeply conserved mammalian and Zoonomia elements, aligning with previous observations of fine-mapped eSNVs[48] (Fig. S9). Similarly, candidate causal sc-eTRs were enriched in Zoonomia Group 2 and 3 (actively evolving and primate-specific respectively) cCREs (Fig. S9).

The association between regulatory potential and primate-specific constraint showed marked GC-content dependence, consistent with TFBS and open chromatin regions being on average GC-rich[49,50]. Notably, candidate causal sc-eTRs with 61-80% GC content demonstrated the strongest enrichment for TFBS in constrained primate-specific elements (OR = 13.5, Fisher's exact test, $P = 2.47\times10^{-7}$). Higher GC content (81-100%) sc-eTRs exhibited substantial enrichment in DNase hypersensitivity summit sites within constrained primate elements (OR = 2.74, Fisher's exact test, $P = 1.88\times10^{-7}$).

We identified 858 distinct candidate causal sc-eTRs significantly associated with methylation of nearby CpG sites (within 5 kb) using methylation signatures derived from PacBio HiFi sequencing (n=25, Bonferroni-corrected $P < 0.05$, Table S4). On average, each candidate causal sc-eTR associated with approximately two nearby CpG sites (standard error = 0.075). Compared to all TRs genotyped, candidate causal sc-eTRs associating with methylation were significantly enriched in promoter, 3' UTR, and intronic regions (OR = 4.2, 2.7, 1.7, Fisher's exact test, $P = 6.70\times10^{-16}$, 5.95×10^{-8}, 1.72×10^{-27} respectively); they were negatively enriched in intergenic regions (OR = 0.51, Fisher's exact test, $P = 9.24\times10^{-44}$). Increasing repeat length tended to associate with increased methylation (median effect size = 0.35, Wilcoxon signed-rank test, $P = 1.63\times10^{-8}$).

Direct genotyping of TR loci revealed several novel fine-mapped associations, with candidate causal sc-eTRs exhibiting weak to moderate linkage disequilibrium with the lead SNV of the respective *cis* window (median $r^2 = 0.34$, interquartile range [IQR] = 0.085-0.61) (Fig. 3b). Approximately 29% of candidate causal sc-eTRs remained significant ($P < 5\times10^{-8}$) after conditioning on the genotype of the lead SNV, suggesting that a subset of these sc-eTRs may explain additional variation in gene expression beyond what can be explained by SNVs alone (Table S5).

For instance, we found a CTCF-binding poly(GTGC) 5' UTR repeat to be candidate causal for *RUNDC3B* expression in 9 lymphoid cell types (minimum $P = 4.9\times10^{-82}$, Fig. 3c). Previous work has shown that *RUNDC3B* promoter methylation is specific to lymphoid cell lines, and absent in myeloid lineages[51]. As another example, we identified a poly(A) repeat as candidate causal for *IFNAR1* expression in $CD4_{TCM}$ cells ($P = 6.92\times10^{-94}$, Fig. 3d). *IFNAR1* encodes a receptor for interferon alpha and beta, signaling molecules important for modulating T cell function[52]. One of the strongest signals we observed was a poly(GCTCCGGAATCCGGTGCGGAGGCTTGG) repeat in the 5' UTR of *PLA2G4C*, specific to B-cells (minimum $P = 9.61\times10^{-216}$, Fig. 3e). PLA2G4C hydrolyses glycerophospholipids, releasing free fatty acids and other lipids to be used as precursors for signaling molecules[53].

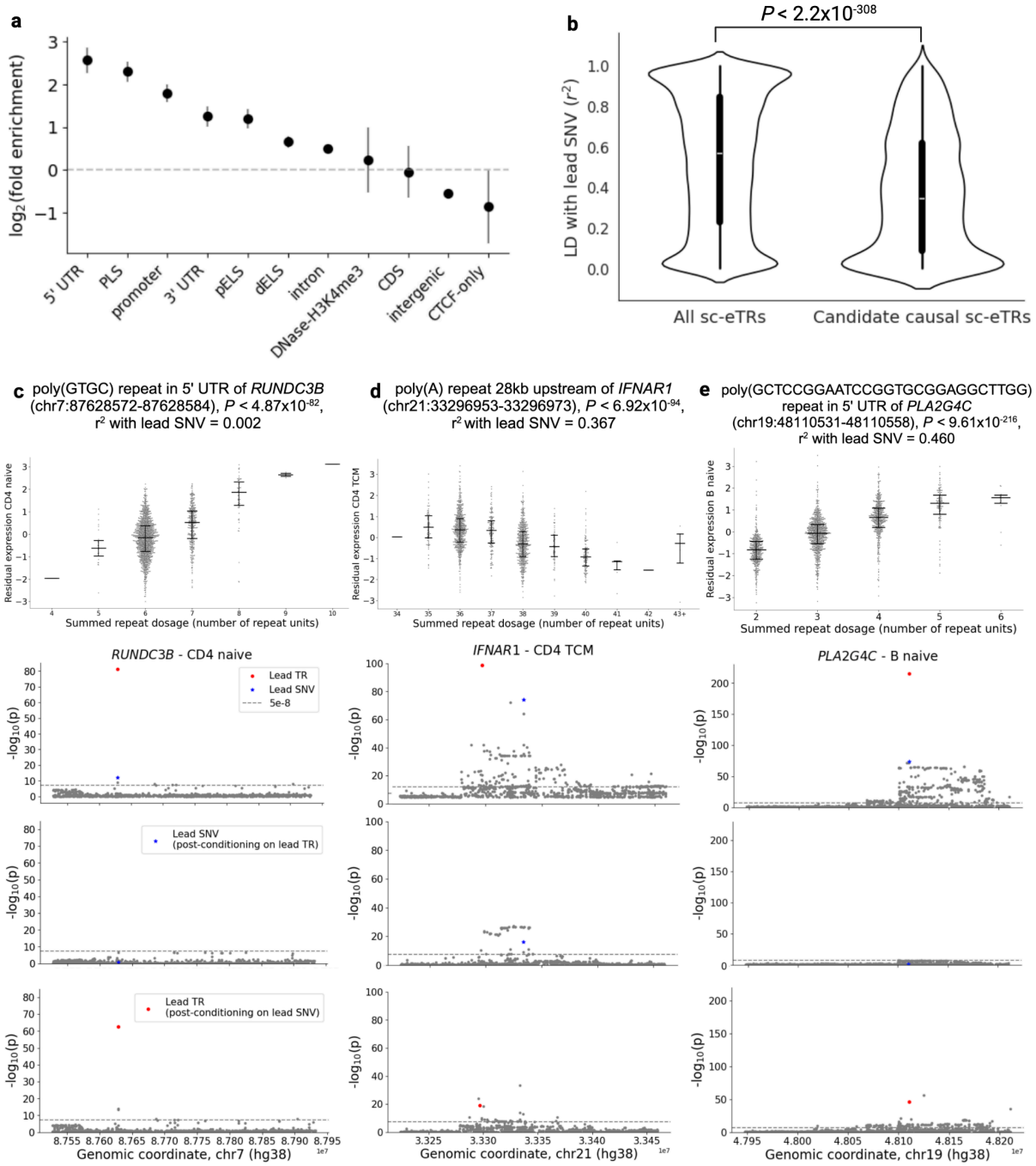

Figure 3: Characterization of candidate causal sc-eTRs. a, Functional enrichment of candidate causal sc-eTR relative to all TRs genotyped. The y axis denotes $\log_2$fold enrichment, comparing candidate causal sc-eTRs to all TRs genotyped. Error bars correspond to 95% confidence intervals. ENCODE candidate *cis* regulatory element (cCRE) annotations are abbreviated as follows: promoter-like signature [PLS], proximal enhancer-like signature [pELS], distal enhancer-like signature [dELS], CTCF binding site failing to intersect another cCRE annotation [CTCF-only]. **b**, Distribution of linkage disequilibrium (LD) with the lead SNV of the respective *cis* window for all sc-eTRs and for candidate causal sc-eTRs. Violin plots summarize the distribution of effect sizes with horizontal lines showing median values and boxes spanning from the 25th (Q1) to the 75th percentile (Q3). Whiskers extend to Q1 - 1.5 x IQR and Q3 + 1.5 x IQR, where IQR is the interquartile range. **c-e**, Case examples of candidate causal sc-eTRs. For each locus, the upper plot shows the association between repeat length and residual gene expression, while the remaining plots show the results of the association analysis, conditional analysis on the genotype of the candidate causal sc-eTR, and

conditional analysis on the genotype of the lead SNV. In detail, the second plot shows the original association signals for the candidate causal sc-eTR (red circle), the lead eSNV (blue star), and other SNVs and TRs within +/- 100kb of the gene body (gray points). The third plot shows the association signals for the same set of variants, conditioning each on the summed genotype of the candidate causal sc-eTR. The fourth plot shows the association signals for the same set of variants, conditioning each on the genotype of the lead eSNV.

While rare repeat expansions in over 60 TR loci have been identified as causal for severe monogenic disorders[54], the impact of common variation at these loci is less understood[55]. Surprisingly, given most disease-associated TRs act through neuronal pathways[8] and are not known to have biological impact in blood cells, common TR variation was found to nominally associate with gene expression across all 46 known disease-associated loci that passed QC (uncorrected $P < 0.05$). In 5 of these loci - *C9orf72*, *GLS*, *PPP2R2B*, *FRA10AC1*, and *DIP2B* - common TR variation was identified as candidate causal for gene expression (Table S6, Note S4).

We considered how candidate causal sc-eTRs could annotate disease-associated genes lacking known TR-mediated mechanisms. We hypothesized that TR length variation could contribute to variable penetrance of pathogenic variants in *cis*, mask causative dominant variants in autosomal dominant haploinsufficient genes in *trans*, or act as a 'second hit' in a recessive gene with one candidate pathogenic variant. We found that 24.7% of eGenes associated with candidate causal sc-eTRs were represented in PanelApp[56], a public database of gene panels for human disorders (Table S7), highlighting a subset of loci that warrant further exploration in disease cohorts.

Candidate causal sc-eTRs likely drive complex traits

We subsequently investigated whether candidate causal sc-eTRs could help explain variation in complex traits. We first intersected candidate causal sc-eTRs with significant TR PheWAS hits from UK Biobank (UKBB) (Fig. 4a, Table S8, Methods). Candidate causal sc-eTRs associating with hematological traits were enriched in 5' UTR and promoter regions, compared to all candidate causal sc-eTRs (OR = 18.0, 6.4, Fisher's exact test, $P = 5.3\times10^{-14}$ and $= 1.9\times10^{-6}$ respectively, Fig. S10).

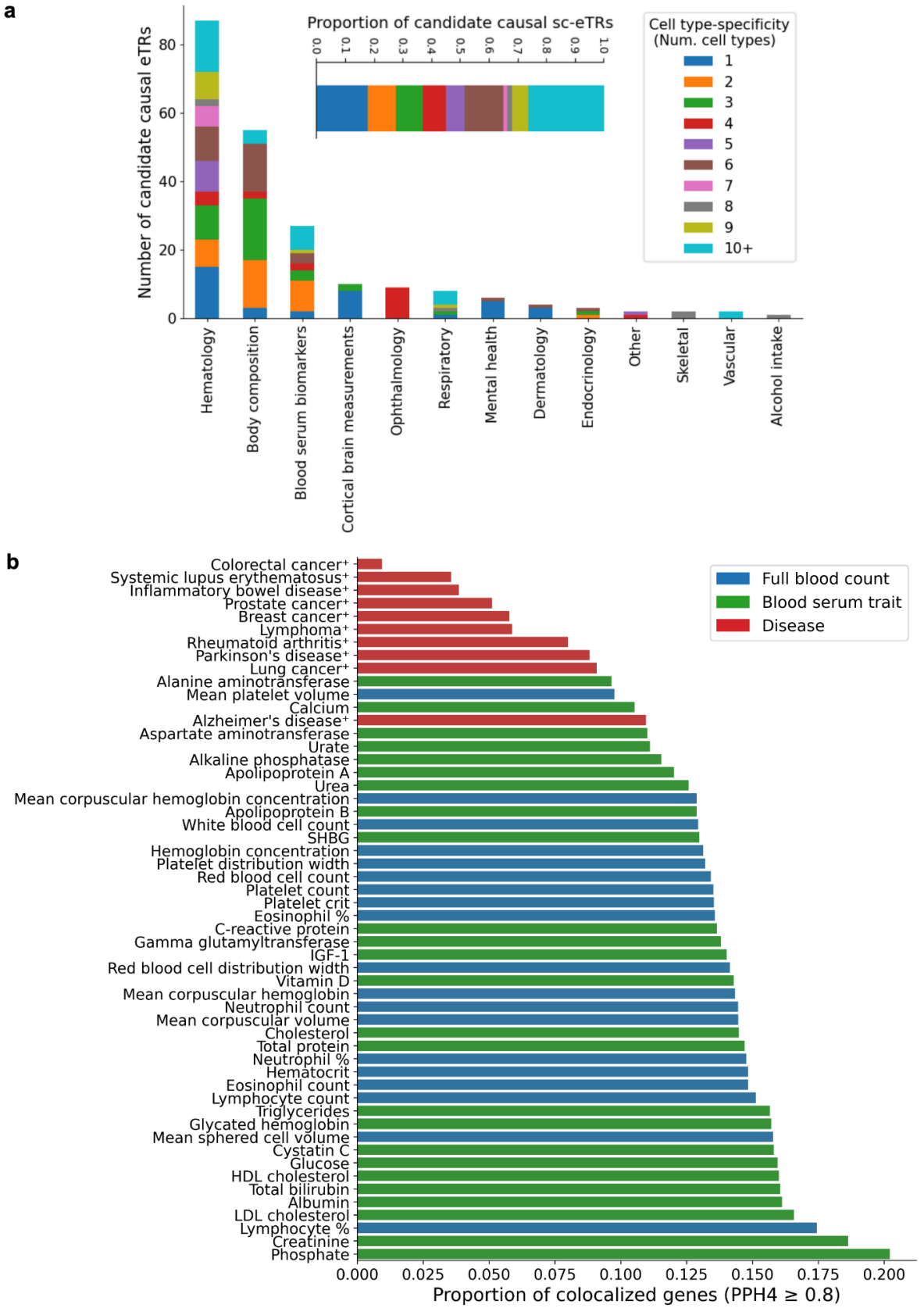

Figure 4: Candidate causal sc-eTRs associate with complex trait variation.
a, Barplot of the number of candidate causal sc-eTRs intersecting TR UKBB PheWAS hits, colored by cell type specificity. **b,** Barplot of the proportion of colocalized genes (PPH4 ≥0.8) containing a

candidate causal sc-eTR relative to all genes tested for colocalization, per GWAS catalog. Phenotypes marked with † were colocalized using only SNVs while unmarked phenotypes were colocalized using SNVs and imputed TRs.

We then performed colocalization analysis to compare our sc-eQTL (sc-eSNV+sc-eTR) data with existing GWAS catalogs. The goal of colocalization is to determine whether a common genetic variant is likely to influence both gene expression and a complex trait, thereby providing insights into the biological mechanisms underlying associations observed in GWAS. We performed colocalization with two types of catalogs: (1) SNV-only GWAS catalogs for autoimmune conditions (inflammatory bowel disease [IBD][57], rheumatoid arthritis[58], systemic lupus erythematosus[59]), cancer (breast[60], colorectal[61], lung[62], lymphoma[63], prostate[64]), COVID-19[65], and neuroinflammatory conditions (Alzheimer's[66] and Parkinson's disease[67]); and (2) joint SNV and imputed STR GWAS catalogs for 44 UKBB blood serum and full blood count traits[11] (Fig. 4b).

We hypothesized that candidate causal sc-eTRs could drive GWAS signals if the following conditions were met: (1) strong colocalization indicating that the trait and gene expression are driven by the same variant (PP H4 $\geq$ 0.8), (2) evidence that the sc-eTR is the lead variant driving changes in gene expression and is confidently fine-mapped (PIP $\geq$ 0.7 using a single causal variant model), and (3) evidence that the sc-eTR is in at least moderate linkage disequilibrium (LD, $r^2 \geq 0.5$) with a variant cataloged in the GWAS.

For each trait, we restricted colocalization to eGenes that contained at least one candidate causal sc-eTR ($P < 5\times10^{-8}$) within 100 kb of the gene body, and that had at least one genome-wide significant ($P < 5\times10^{-8}$) signal within the same window in the GWAS catalog. In our sc-eQTL dataset, we identified a mean of 1,672 genes per cell type containing at least one significant ($P < 5\times10^{-8}$) signal, of which 80.3% were tagged by both significant sc-eSNV and sc-eTR signals, 16.8% were tagged by significant sc-eSNV signals only, and 2.9% were tagged by significant sc-eTR signals only. We then used coloc[68] to compute the probability that the trait and expression of the gene were driven by the same variant, testing a total of 19,678 gene-trait pairs (Methods).

We identified 2,040 GWAS loci where the candidate causal sc-eTR was in at least moderate LD ($r^2 \geq 0.5$) with a variant in the GWAS catalog, and there was strong evidence that the trait and expression of the gene were driven by the same variant (PP H4 $\geq$ 0.8) (Table S9). Generally, the greatest number of colocalizations was observed for full blood count (FBC) traits, followed by blood serum traits, and finally disease phenotypes, likely reflecting both the relative order of impact of gene expression and extent of polygenic contribution to these traits. Controlling for polygenic contribution, the proportion of genes tested with strong colocalization evidence (PP H4 $\geq$ 0.8) varied by trait, with 17.4% of loci colocalizing for lymphocyte percentage and 11% for Alzheimer's disease (Fig. 4b).

As an example, we found a poly(T) candidate causal sc-eTR in the promoter of *KIF16B* strongly colocalizing with mean platelet volume in cytotoxic immune cells ($CD4_{CTL}$, NK subtypes, $CD8_{TEM}$, and CD8+ naive) (maximum PP H4 = 1; minimum $P < 2.2\times10^{-308}$). *KIF16B* encodes a kinesin motor protein, which transports intracellular signaling molecules to the cell membrane[69]. Kinesin proteins have been found to regulate pro-inflammatory α-granule and dense granule secretion in platelets[70] and have also been found to influence lytic granule

secretion in T[71] and NK cells[72]. Our results suggest that *KIF16B* may be involved in the immunological synapse between cytotoxic cells and platelets during pro-inflammatory states[73].

The cell type specificity of our dataset also allows for further contextualization of sc-eTRs in relation to disease. We found that a poly(GCC) sc-eTR in the 5' UTR of *BCL2L11,* previously associated with eosinophil count, monocyte count, and other inflammatory markers[11,14], is significant in CD4+ naive T cells, and strongly colocalizes with IBD (PP H4 = 0.99, P = 6.13×10^{-12}, Fig. 5). *BCL2L11* expression has been previously established to regulate the lifespan of CD4+ naive T cells[74,75]. Moreover, CD4+ T cells are enriched in IBD lesions, with CD4+ T cell-blocking antibodies effective in inducing remission in some cases[76]. The identification of this CD4+ naive T cell-specific eTR may provide mechanistic insight into IBD pathogenesis, warranting further functional validation to assess its potential as a cell type-specific therapeutic target.

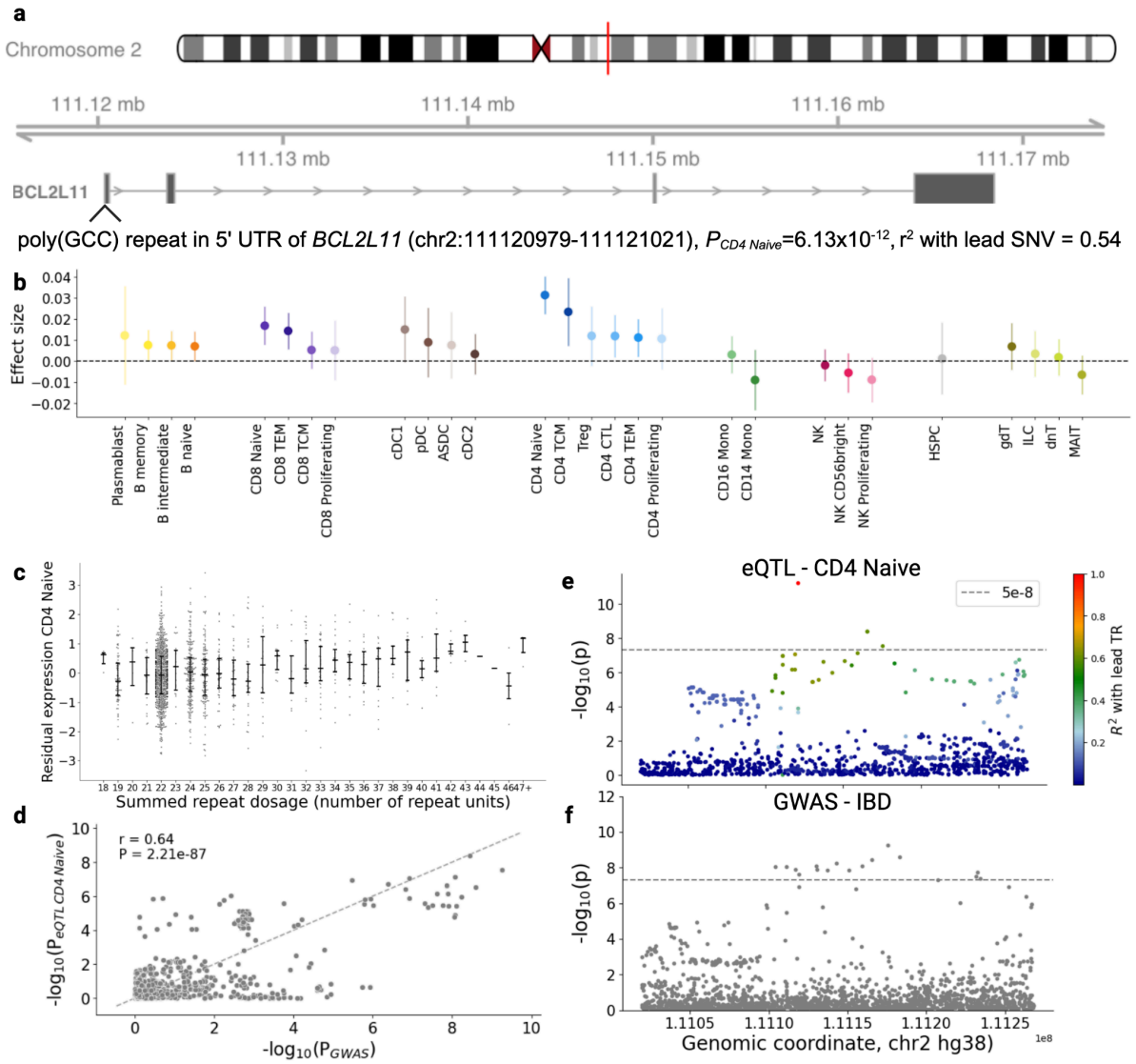

Figure 5: poly(GCC) repeat in the 5' UTR of *BCL2L11* colocalizes with GWAS for inflammatory bowel disease (IBD). a, Locus zoom plot of *BCL2L11* using Gviz[77], loaded with GENCODE v44 track**.** **b**, Distribution of effect size of the sc-eTR in 28 immune cell types. Error bars correspond to 95%

confidence intervals. **c**, Association between repeat length and residual gene expression in CD4+ naive T cells. **d**, Association between p-values of overlapping variants in the CD4+ naive T cell sc-eQTL dataset and IBD GWAS catalog[57]. **e**, sc-eQTL association signals for the candidate causal sc-eTR (red circle) and other SNVs and TRs within +/- 100kb of the gene body, colored by strength of linkage disequilibrium with the candidate causal TR (R^2). **f**, IBD GWAS association signals for the equivalent window (+/- 100kB of the gene body of *BCL2L11*).

We also found a monocyte-specific poly(GCG) eTR in the 5' UTR of *FAM117B* strongly colocalizing with apolipoprotein A and HDL cholesterol (PP H4 = 0.96, 0.92 respectively; minimum $P = 5.33\text{x}10^{-94}$). FAM117B is known to activate the KEAP1/NRF2 pathway[78], a key regulator of cholesterol metabolism[79]. Both HDL cholesterol and apolipoprotein A - a major component of HDL cholesterol - have been demonstrated to inhibit monocyte foam cell formation[80] and chemotaxis[81], delaying atherosclerotic plaque progression. Functional validation of this monocyte-specific eTR may uncover new insights on modulating atherosclerosis.

In addition, we observed a naive B cell type-specific poly(T) eTR in a promoter-like signature roughly 5 kb upstream of *CCR6* strongly colocalizing with rheumatoid arthritis, neutrophil percent, and total protein (PP H4 = 0.99, 0.94, 0.92 respectively, $P = 3.8\times10^{-35}$). CCR6 is a chemokine receptor that regulates Th17 migration[82] and marks memory B cell precursors[83]. Individuals with rheumatoid arthritis have been found to have increased levels of B cells expressing *CCR6*, with the shift predominantly occurring in the naive B cell subset[84]. CCR6 binds to ligand CCL20, triggering an inflammatory cascade involving neutrophil recruitment[85] and changes in acute phase protein concentrations, consistent with our colocalization findings.

Discussion

Our genome-wide analysis of TRs across 28 circulating immune cell types unveils a landscape of over 58,000 unique *cis*-acting single-cell expression quantitative trait TR loci (sc-eTRs), demonstrating the remarkable regulatory potential of repeat sequences. We conservatively identified 6,210 candidate causal sc-eTRs, which generally showed weak linkage disequilibrium (LD) with the lead SNV of their respective loci. Our work challenges the traditional paradigms of SNV- and imputation-based eQTL mapping by demonstrating that direct TR genotyping is essential for accurately capturing their unique contributions to gene expression variation.

Our findings reveal important insights into TRs as context-sensitive modulators of gene expression. We propose that some TRs can function both as continuous modulators and binary switches, a duality that challenges the assumptions of most eQTL models, including our own. For instance, at the *FRA10AC1* locus, we observed that repeat length positively associates with gene expression within the spectrum of common variation tested in our study, while larger pathogenic expansions have been reported to induce gene silencing[86]. This non-linear relationship may be more widespread, emphasizing the need to assess both the magnitude and direction of sc-eTR effects across the entire repeat length spectrum and in different cellular contexts. Indeed, some sc-eTRs achieving statistical significance across multiple cell types may appear shared but can still exert distinct, cell type-specific effects on expression.

Our work demonstrates the value of including epigenetic analysis to understand how TRs modulate gene expression. Although repeat expansions have been widely associated with gene silencing via epigenetic modifications[87,88], our genome-wide analysis expands the catalog of cases where increasing TR length can often increase the expression of nearby genes[9]. Future epigenetic studies with larger sample sizes will help elucidate these mechanisms.

The substantial number of novel sc-eTR associations we discovered underscores the need for directly genotyped repeat-inclusive genomic catalogs to perform downstream analysis currently out of reach, such as Mendelian randomization. Availability of these resources will also improve the power and sensitivity of existing analyses, allowing us to colocalize loci even when the finemapped TR is not well tagged by neighboring SNVs.

Despite computational advances, genotyping uncertainty remains a challenge as current short-read sequencing technologies still struggle to accurately capture subsets of TR variation, including repeats found in low complexity regions (Note S1). Long-read sequencing holds promise for improving genotyping accuracy. Identifying contexts in which short-read sequencing is sufficient and those where the additional resolution of long-read sequencing is helpful will optimize the application of long-read sequencing in population-scale studies.

Moreover, our work highlights ongoing challenges in modeling TR variation, which include both stepwise mutations and repeat instability of large expansions[89]. Addressing these challenges will require continued refinement of analytical tools, such as considering both germline and somatic mutation models, as well as evaluating allele-specific effects on gene expression variation. Wet laboratory validation of *in silico* findings remains paramount with advances in high-throughput CRISPR screening and synthetic biology approaches[90] offering exciting opportunities to systematically validate the functional impact of TRs in relevant cellular contexts.

In conclusion, this work shows that TRs exert substantial effects on cell type-specific gene expression, and that direct analysis of this class of variation is an important complement to SNV-centric approaches for deciphering genetic regulation. Future efforts toward a more comprehensive genomics approach—integrating diverse forms of genetic variation, from single nucleotides to complex structural variants, alongside epigenetic and environmental factors—will provide valuable insights into human biology, disease etiology, and therapeutic development.

Methods

TenK10K Phase 1 dataset processing

The TenK10K Phase 1 resource, including sample quality control, WGS and single-cell RNA processing, will be described in more detail in an upcoming preprint by Cuomo et al. Phase 1 of TenK10K consists of the Tasmanian Ophthalmic Biobank cohort (964 European ancestry individuals with no signs of ocular disease) and the BioHEART cohort (826 European ancestry individuals with diagnosed or suspected cardiac disorders). In brief, we collected peripheral blood from 2,045 individuals. Tasmanian Ophthalmic Biobank samples were

prepared for sequencing using the KAPA Hyper PCR-free sequencing library preparation kit (Roche) while BioHEART samples were prepared using the DNA PCR-free sequencing library preparation kit (Illumina).

Samples underwent short-read WGS (30x) using the Illumina NovaSeq 6000 platform (2 x 150bp) and were aligned to hg38 using DRAGMAP (v1.3.0), as per DRAGEN-GATK best practices. To generate scRNA-seq data, peripheral blood mononuclear cells were isolated from each sample before undergoing single-cell RNA capture and barcoding (10x Genomics), multiplex sequencing using Illumina NovaSeq 6000 platform, alignment to genome reference (hg38, Gencode release 44, Ensembl 110) using STAR[91], and demultiplexing with vireo[92] (v2.1.0) in the Demuxafy implementation. Poor genotyping and/or sample quality, cryptic relatedness, and ancestral outliers were removed, resulting in 1,790 individuals with paired WGS and scRNA-seq data.

This study complied with all relevant ethical regulations and was overseen by the Human Research Ethics Committees at the Royal Children's Hospital (Melbourne, Australia), Northern Sydney Local Health District (Sydney, Australia), St. Vincent's Hospital (Sydney, Australia), and University of Tasmania (Hobart, Australia). Informed consent was obtained from all participants.

TR catalog curation

A catalog of 4,918,794 loci was generated by merging several existing catalogs: disease-associated loci (72 loci)[93], v17 hg38 reference file from GangSTR (1,340,266 loci)[22], hg38 reference file from HipSTR (1,634,957 loci)[23], Illumina's polymorphic catalog based on the 1000 Genomes Project (174,293 loci)[25], hg38 reference file from TRGT (171,146 loci)[28], polymorphic catalog of TR loci based on 51 haplotype-resolved assemblies from the Human Pangenome Reference Consortium (1,573,403 loci)[26,28], and a catalog generated by Tandem Repeat Finder (TRF)[21] (v4.09) consisting of TR loci in hg38 that span at least 9bp. The TRF catalog was generated using the following settings: match = 2, mismatch = 7, indel penalty = 1000000, PM = 80, PI = 10, minscore = 8, and maxperiod = 2000.

Merging of the TR catalogs is fully described in a separate manuscript by Weisburd and Dolzhenko et al.[27]. Briefly, component catalogs were parsed sequentially, and additional loci were added to the final catalog unless their coordinates overlapped existing included loci by 66% or more and had the same motif. Finally, to improve local read alignment for TR loci with nearby repeats, locus definitions in the catalog were modified to include adjacent repeats, if any, resulting in compound locus definitions (locus definitions with more than one TR variant specified). Compound locus definitions include a maximum of 3 TRs which are separated from each other by no more than 6bp.

Polymorphic TR catalog curation

TR loci must be polymorphic in order for an association to exist between changes in repeat length and gene expression. To identify polymorphic TR loci in the cohort, ExpansionHunter (v5)[31] (threads = 16, analysis-mode = streaming) was run using the aforementioned genome-wide catalog on 200 randomly selected 'XX' individuals.

Using Hail Query v0.2.126 (https://github.com/hail-is/hail), we removed chrY, chrM, and monomorphic loci from the resulting VCF, producing a polymorphic catalog of 2,638,529 loci (Supplementary Files).

Benchmarking against Simons Genome Diversity Project (SGDP) samples

The performance of ExpansionHunter (v5)[31], GangSTR (v2.5)[22], and HipSTR (v0.6.2)[23] were benchmarked using capillary electrophoresis results of hypervariable microsatellite loci. Specifically, WGS data and capillary electrophoresis results of 120 samples from the Simons Genome Diversity Project (SGDP) were downloaded from publicly accessible websites[33]. FASTQ files were downloaded from ENA Archive (accession no. ERP010710) and aligned to hg38 reference genome with DRAGMAP (https://github.com/Illumina/DRAGMAP), according to National Approach to Genomic Information Management (NAGIM) guidelines (https://queenslandgenomics.org/qldgenomics-updated/wp-content/uploads/2021/02/NAGIM-Blueprint-v20201010-Final-v1.2.2.pdf). Capillary electrophoresis results (in bp) corresponding to 627 STR loci were downloaded from (https://web.stanford.edu/group/rosenberglab/data/pembertonEtAl2009/combinedmicrosats_627loci_1048indivs_numRpts.stru). Primer sequences and the repeat motif of each target PCR amplicon were downloaded from (https://web.stanford.edu/group/rosenberglab/data/pembertonEtAl2009/Pemberton_AdditionalFile1_11242009.txt). We filtered for motif structures that were simple (consisting of one motif) and pure (without any sequence interruptions), resulting in a subset of 482 loci. Primer sequences of the selected loci were then mapped to hg38 reference genome using *in silico* PCR[94]. 94 loci were removed from the dataset as primer sequences could not be mapped to hg38. This produced a PCR validation dataset of 388 STR loci.

To confirm the TR motif, the number of repeat copies found in the reference genome, and the coordinates of each TR locus, TandemRepeatFinder[21] was run on each target PCR amplicon using the settings match = 2, mismatch = 30, delta = 30, PM = 80, PI = 10, minscore = 16, maxperiod = 2000. TR loci initially defined on the antisense strand were further processed by taking the reverse complement of the sequence and re-performing TandemRepeatFinder to standardize all TR locus definitions by the sense strand.

To calculate the repeat copy allele from the PCR base pair result, the following formula was used at each TR locus: $c = r + (w - l)/s$, where *c* is the repeat copy, *r* is the number of repeats in hg38, *w* is the PCR amplified fragment (bp), *l* is the length of the PCR amplicon (bp) in hg38, and *s* is the motif length (bp) of the target TR[95]. Repeat copy alleles were rounded down to the nearest whole number. PCR genotypes were masked for a sample at a particular locus if an indel was identified within the PCR target region but outside of the TR locus. Indels were identified using publicly accessible FermiKit calls (https://github.com/lh3/sgdp-fermi).

Using the coordinates of each TR locus, hg38 variant catalogs were created for ExpansionHunter, GangSTR, and HipSTR. All three callers were used to genotype 120 WGS samples. ExpansionHunter was run with --analysis-mode = streaming and --threads = 16 options. GangSTR was run using default parameters. HipSTR was run using the joint calling option.

In a subset of loci, non-zero offsets were applied to correct the PCR-derived repeat copy alleles. We followed a previously published protocol where, at each locus, every discordant call made by a TR caller relative to the PCR-derived genotype was recorded and the magnitude of the discordance was scored[96]. The offset was scored as a 1 if applying the offset to the genotype produced by the TR caller recovered both PCR-derived alleles. A score of 0.5 was given if the genotype produced by the TR caller was homozygous but applying the offset recovered only one PCR-derived allele. Lastly, a score of 0.25 was given if the genotype produced by the TR caller was heterozygous but the offset recovered only one PCR-derived allele. At each locus, offset calculations were calculated separately for each of the three TR callers. Only loci with at least 20 calls were considered. An offset was applied to the PCR-derived genotype only if it was the highest-ranking offset in calls made by all three TR callers at a particular locus.

Validation with long-read sequencing

HiFi sequencing methods

Cells frozen in 90% FBS:10% DMSO were defrosted at room temperature. The cells were pelleted at 4°C, 500g for 5 minutes, washed with 100 µL of 1x PBS, and then pelleted again under the same conditions. The supernatant was discarded, and the pellet was processed immediately using the Nanobind CBB DNA extraction kit (102-301-900, PacBio). Cell counts ranged from 1.6 to 4.22 x 10^6 cells, and extracted DNA was eluted in 150 µL of EB buffer.

DNA samples were homogenized using a Diagenode Megaruptor with the 3 DNAFluid+ Kit (E07020001, Diagenode) under the following conditions: volume 150 µL, speed 40, and concentration 50 ng/µL. Subsequently, 3 µg of material was diluted in low TE to a final volume of 130 µL. Shearing was performed with the Megaruptor shearing kit (E07010003, Diagenode) at speed 30 or 31, aiming for average fragment lengths of 15–24 kb. Clean-up and concentration of the sheared material were conducted using SMRTbell clean-up beads (102-158-300, PacBio), and the DNA was eluted in 47 µL. Average fragment lengths were determined using the Femto Pulse system with the Genomic DNA 165kb Analysis Kit (FP-1002-0275, Agilent).

SMRTbell libraries were prepared using the SMRTbell® Prep Kit 3.0 (102-141-700, PacBio) following standard procedures, including unique barcoding of each sample with the SMRTbell Adapter Index Plate 96A (102-009-200, PacBio). Size selection was performed with AMPure PB beads (102-182-500, PacBio) at a 2.9x ratio. Final library sizes were confirmed with the Femto Pulse, and libraries were diluted to below 60 ng/µL before the ABC loading procedure. SMRT library fragment lengths ranged between 12.895 and 26.001 kb. Sequencing was performed using the following PacBio products: Revio sequencing plate (02-587-400), Revio Polymerase kit (102-739-100), and Revio SMRT cell tray (102-202-200). On-plate loading concentration was set to 250 pM, with 30-hour movie times. SMRT libraries that did not yield 90 Gb using one SMRT cell were pooled for additional sequencing in "top-up" runs.

Alignment & TR genotyping

The resulting uBAM files were aligned to the hg38 reference genome using minimap2 (v2.28-r1209) with the following parameters: -y --secondary=no --MD -a -x map-hifi. Tandem repeats were genotyped in individual samples using TRGT (v1.1.0) with a custom catalog of polymorphic tandem repeats. The resulting tandem repeat genotypes were then merged into a single VCF for downstream analysis, also using TRGT.

TR genotyping and filtering

ExpansionHunter (v5) was used to genotype TRs defined in the polymorphic TR catalog, producing a diploid TR genotype (in repeat lengths) for each sample using realigned reads. VCFs were merged using mergeSTR (TRTools v5.0.2)[97] and filtered to exclude loci meeting the following criteria: locus-level call rate < 90%, observed heterozygosity < 0.00995 (corresponds to a non-major allele frequency < 0.5%), locus-level Hardy-Weinberg equilibrium (binomial test, $P < 1\times10^{-6}$). Calls that were more than 30 repeats less or 20 repeats greater than the mode allele at a particular locus were set to missing. This threshold was determined based on comparisons with a publicly available truth set[26] to assess genotyping accuracy. All samples had a sample-level TR call rate greater than 99%.

SNV genotyping and filtering

Single nucleotide variants, inclusive of single base substitutions and indels, were genotyped using GATK4 HaplotypeCaller (v4.2.6.1). We removed monomorphic and rare variants, defined as having a minor allele frequency < 1%. Multiallelic variants were split into biallelic variants.

eTR and eSNV association analysis

To study the effect of TR repeat length variation on gene expression in a cell-type specific context, we performed sc-eTR discovery with associaTR (TRTools v5.0.2)[97], a TR-aware association testing framework that performs length-based tests for multiallelic TR loci against a continuous phenotype.

Prior to sc-eTR discovery, scRNA-seq data was processed using approaches that will be described in more detail in an upcoming preprint by Cuomo et al. Briefly, we removed cells that were unassigned to individuals or classified as doublets by at least two out of the three methods: scds[98], vireo[99], and scDblFinder[100]. We also filtered out cells with at least 20% mitochondrial gene expression, those with fewer than 200 expressed genes, and those with more than 6,000 expressed genes to exclude potential doublets and low-quality cells.

scRNA transcript counts were then further processed to generate pseudobulk samples. In detail, single-cell-level normalization was performed using scanpy[101] (v1.9.3) - raw transcript counts were normalized for sequencing depth, log-transformed, and corrected for batch effects - prior to mean aggregation at the sample level. This workflow aligned with the recommendations by Cuomo et al.[102] for optimizing pseudobulk eQTL mapping workflows.

Subsequently, lowly expressed genes (expressed in fewer than 1% of cells) were excluded from each cell type. Expression values for remaining genes were quantile-normalized to a standard normal distribution prior to eQTL mapping.

Expression values were adjusted separately for each cell type to control for karyotypic sex, age, population structure, and technical variation in expression . For population structure, we selected the top 4 principal components (PCs) produced from the principal component analysis of TR genotypes across approximately 1.7 million variable variant sites. Variants are chosen based on the following criteria: are autosomal, have a non-major allele frequency of at least 0.5%, have a call rate of at least 90%, and have a locus-level Hardy-Weinberg equilibrium binomial two-sided $P \geq 1x10^{-6}$.

To control for technical variation in gene expression, we used the top 7 PCs produced from the principal component analysis of mean aggregated normalized RNA transcript counts per cell type. We tested the effect of 1-10 principal components sequentially by adding them one at a time into a linear regression model of $CD8_{TEM}$ *cis* sc-eTR analysis and identified that a model consisting of 7 PCs identified the greatest number of eGenes (Fig. S11)

For each TR within 100 kb of a gene, we used associaTR (TRTools v5.0.2) to perform ordinary least squares regression between the summed TR repeat length (across both alleles for each individual) and normalized gene expression, while adjusting for known confounders:

$$y = W\alpha + g\beta + \epsilon$$

where y denotes normalized gene expression values, W denotes the aforementioned covariates, β denotes the effect size the model is estimating, g denotes the summed TR repeat length, and ϵ is the normally distributed error term. We used the same model for association testing of SNVs and indels within 100kb of each gene, with g denoting the dosage of the non-reference allele.

Meta-analysis

Meta-analysis was performed using a random effects (Dersimonian and Laird) model using the meta package in R (v4.0.0)[103]. To assess potential inflation of Type 1 error, we performed 5 permutations of the sample identifiers in the $CD4_{TCM}$ subtype and repeated the regression analysis. For each of the 5 iterations of permutation, a meta-analysis was performed across the 2 cohorts. We found that Type 1 error was well controlled (Fig. 2a).

Multiple testing correction

Gene level p-values were computed by combining variant-level p-values of variants using the ACAT-V test[104] based on the Cauchy combination. We identified a set of top sc-eTRs by selecting the eTR with the lowest nominal p-value for each gene in each cell type. We then corrected for multiple testing across all genes tested, for every cell type, using the Storey q-value procedure[105], reporting results at FDR < 5%. Original p-values accompany case examples discussed in the main text of the manuscript, with the minimum original p-value provided if the sc-eTR was shared across multiple cell types.

Multivariate adaptive shrinkage (mash) analysis

To account for global effect size sharing and power differences across cell types, we ran mashR (v0.2.79)[35], a multivariate adaptive shrinkage method, following the documentation for eQTL analysis (https://stephenslab.github.io/mashr/articles/eQTL_outline.html). Briefly, we obtained the effect sizes and standard errors for every sc-eTR (FDR <5%) that was tested in every cell type. We used the sc-eTRs to compute the 'data-driven' covariance matrix using an extreme deconvolution method involving the top five principal components. The 'data-driven' and 'canonical' covariance matrices were then used to fit the mash model to all chr22 variants tested in all cell types ('random' tests). Finally, the mash model was used to calculate the posterior effect sizes of sc-eTRs across all cell types.

Cell type specificity analysis

Cell type specificity of sc-eTRs was assessed using a pairwise meta-analysis approach. For each significant sc-eTR (FDR < 5%), we conducted pairwise meta-analyses comparing its effect size in the original cell type to its effect sizes in each of the other cell types.

Meta-analysis was performed using a random effects (Dersimonian and Laird) model with the meta package in R (v4.0.0)[103]. We compared the resulting meta-analysis p-value to the original p-value obtained from the single-cell eQTL analysis. If the meta-analysis p-value was lower than the original p-value, we concluded that the sc-eTR was shared between the two cell types.

To determine cell type specificity, we examined the results of all pairwise comparisons for each sc-eTR. An sc-eTR was considered cell type-specific if the meta-analysis p-value was consistently higher than the original p-value across all cell types where the gene was expressed in at least 1% of cells.

Fine-mapping and conditional analysis

Prior to fine-mapping, we identified and removed indels that represent TR alleles, similar to Margoliash et al[11]. We excluded indels that were 1) found in TR intervals (as defined in our catalog) and 2) composed of whole copies of the TR motif, including its cyclical representations. Conservatively, we retained indels that were not perfect multiples of the TR motif and also retained indels where at least one base would represent a sequence impurity in the TR interval.

We fine-mapped each eGene passing multiple testing correction (FDR < 5%) using SuSiE-RSS (v0.12.35)[106]. The fine-mapping region for each gene was defined as the window extending 100 kilobases (kb) upstream of the transcription start site (TSS) and 100 kb downstream of the transcription end site (TES). To reduce computational burden, we only included variants in the fine-mapping analysis if they had a p-value ≤ $5x10^{-4}$. We used the summary association statistics derived from meta-analysis and restricted SuSiE-RSS to identify a maximum of one causal credible set in all runs. We used SuSIE's posterior inclusion probability (PIP) with non-default parameter prune_by_cs set to TRUE, as per Margoliash et al[11]. We conservatively considered an sc-eTR to be candidate causal if it was the strongest signal in the eGene and had a SuSIE PIP of at least 0.7. We then performed conditional analysis on every candidate causal sc-eTR by performing association testing as

previously described, conditioned on the summed repeat dosages of the candidate causal sc-eTR.

Functional and genomic annotation of eTRs

We used publicly accessible resources to annotate the sc-eTRs, including ENCODE (v3) *cis* candidate regulatory elements (cCREs) combined from all cell types (https://hgdownload.soe.ucsc.edu/gbdb/hg38/encode3/ccre/encodeCcreCombined.bb), MANE v1.0 (https://ftp.ncbi.nlm.nih.gov/refseq/MANE/MANE_human/), and TR PhEWAS hits[14] (https://www.medrxiv.org/content/10.1101/2024.01.22.24301630v1.supplementary-material [Table S3]).

Methylation analysis

We used pb-CpG-tools (v2.3.2) to obtain site methylation probabilities for all CpG sites genome-wide in 25 PacBio HiFi sequencing samples, corresponding to long-read sequencing of 25 individuals in Phase 1 of TenK10K.

At each CpG site, methylation probabilities were quantile-normalized to a standard normal distribution, and CpG sites were retained for eQTL mapping if the standard deviation of methylation values was greater than 0.02, as per Trujillo et al.[10]

For each candidate causal TR within 5 kb of a CpG site, we used associaTR (TRTools v5.0.2)[97] to perform ordinary least squares regression between the summed TR repeat length (across both alleles for each individual) and normalized methylation probability, while adjusting for known confounders:

$$y = W\alpha + g\beta + \epsilon$$

where y denotes normalized gene expression values, W denotes the aforementioned covariates (karyotypic sex, age, population structure), β denotes the effect size the model is estimating, g denotes the summed TR repeat length, and ϵ is the normally distributed error term.

Bonferroni correction was applied to adjust for the number of TR-CpG pairs tested, with significant associations reported with a Bonferroni-adjusted p-value < 0.05.

Colocalization

We downloaded publicly accessible SNV GWAS summary statistics for inflammatory bowel disease[57] (https://www.dropbox.com/scl/fi/9yyfkpa09x2bm3s56q1t2/liu-2022-east-asian-gwas.tar.gz?rlkey=96ezojmceei0ofe71z3pe7gm3&dl=0), systemic lupus erythematosus[59] (https://www.ebi.ac.uk/gwas/studies/GCST003156), rheumatoid arthritis[58] (https://www.ebi.ac.uk/gwas/studies/GCST90132223), COVID-19[65] (https://www.ebi.ac.uk/gwas/studies/GCST011071), lung cancer[62] (https://www.ebi.ac.uk/gwas/studies/GCST004748), breast cancer[60]

(https://www.ebi.ac.uk/gwas/studies/GCST004988), Parkinson's disease[67] (https://www.ebi.ac.uk/gwas/studies/GCST009325), malignant lymphoma[63] (https://www.ebi.ac.uk/gwas/studies/GCST90018878), prostate cancer[64] (https://www.ebi.ac.uk/gwas/studies/GCST90274713), Alzheimer's disease[66] (https://www.ebi.ac.uk/gwas/studies/GCST90027158), and colorectal cancer[61] (https://www.ebi.ac.uk/gwas/studies/GCST90129505). We downloaded SNV and imputed STR UKBB GWAS summary statistics for 44 blood cell count and serum traits[11] from (https://gymreklab.com/science/2023/09/08/Margoliash-et-al-paper.html).

Colocalization was performed using coloc.abf function from coloc (v5.2.3)[68]. SNV-only colocalization was performed using SNV GWAS summary statistics and sc-eSNVs in our dataset with eQTL type set to 'quant' and sdY = 1 as expression was quantile normalized to a standard normal distribution. Prior to TR and SNV joint colocalization using imputed STR and SNV UKBB GWAS summary statistics, we harmonized the TR locus definitions in the GWAS catalog with those in our TR catalog by verifying, for each pair of intersecting locus definitions, whether one motif was the reverse complement and/or cyclical shift of the other.

Linkage disequilibrium was calculated by taking the square of the Pearson correlation of the genotypes of every pair of variants (summed repeat dosage for TRs or genotype dosage of the non-reference allele for SNVs).

Acknowledgements

We acknowledge Vladislav Savelyev's contribution in developing the prototype whole-genome sequencing production pipeline. We thank Garvan Genomics Platform for providing sequencing services and technical support

Data availability

The polymorphic variant catalog is provided in the supplement.
Summary level association statistics are provided as supplementary files.
Raw summary association statistics are available at 10.5281/zenodo.14010498.

Code availability

The code used for merging and catalog curation is available at https://github.com/broadinstitute/str-analysis.

The TR genotyping, QC, and association analysis pipeline is available at https://github.com/populationgenomics/sv-workflows/tree/main/str.

References

1. Horton, C. A. *et al.* Short tandem repeats bind transcription factors to tune eukaryotic gene expression. *Science* **381**, eadd1250 (2023).

2. Ziaei Jam, H. *et al.* A deep population reference panel of tandem repeat variation. *Nat. Commun.* **14**, 6711 (2023).
3. Sun, J. X. *et al.* A direct characterization of human mutation based on microsatellites. *Nat. Genet.* **44**, 1161–1165 (2012).
4. Gent, J. I. *et al.* Distinct influences of tandem repeats and retrotransposons on CENH3 nucleosome positioning. *Epigenetics Chromatin* **4**, 3 (2011).
5. Vinces, M. D., Legendre, M., Caldara, M., Hagihara, M. & Verstrepen, K. J. Unstable tandem repeats in promoters confer transcriptional evolvability. *Science* **324**, 1213–1216 (2009).
6. Sawaya, S. *et al.* Microsatellite tandem repeats are abundant in human promoters and are associated with regulatory elements. *PLoS One* **8**, e54710 (2013).
7. Tanudisastro, H. A., Deveson, I. W., Dashnow, H. & MacArthur, D. G. Sequencing and characterizing short tandem repeats in the human genome. *Nat. Rev. Genet.* **25**, 460–475 (2024).
8. Depienne, C. & Mandel, J.-L. 30 years of repeat expansion disorders: What have we learned and what are the remaining challenges? *Am. J. Hum. Genet.* **108**, 764–785 (2021).
9. Fotsing, S. F. *et al.* The impact of short tandem repeat variation on gene expression. *Nat. Genet.* **51**, 1652–1659 (2019).
10. Martin-Trujillo, A., Garg, P., Patel, N., Jadhav, B. & Sharp, A. J. Genome-wide evaluation of the effect of short tandem repeat variation on local DNA methylation. *Genome Res.* **33**, 184–196 (2023).
11. Margoliash, J. *et al.* Polymorphic short tandem repeats make widespread contributions to blood and serum traits. *Cell Genom* **3**, 100458 (2023).
12. Erwin, G. S. *et al.* Recurrent repeat expansions in human cancer genomes. *Nature* **613**, 96–102 (2023).
13. Verbiest, M. A. *et al.* Short tandem repeat mutations regulate gene expression in colorectal cancer. *Sci. Rep.* **14**, 3331 (2024).

14. Manigbas, C. A. *et al.* A phenome-wide association study of tandem repeat variation in 168,554 individuals from the UK Biobank. *medRxiv* (2024) doi:10.1101/2024.01.22.24301630.
15. Saini, S., Mitra, I., Mousavi, N., Fotsing, S. F. & Gymrek, M. A reference haplotype panel for genome-wide imputation of short tandem repeats. *Nat. Commun.* **9**, 4397 (2018).
16. Cuomo, A. S. E., Nathan, A., Raychaudhuri, S., MacArthur, D. G. & Powell, J. E. Single-cell genomics meets human genetics. *Nat. Rev. Genet.* **24**, 535–549 (2023).
17. Yazar, S. *et al.* Single-cell eQTL mapping identifies cell type-specific genetic control of autoimmune disease. *Science* **376**, eabf3041 (2022).
18. Cuomo, A. S. E. *et al.* Single-cell RNA-sequencing of differentiating iPS cells reveals dynamic genetic effects on gene expression. *Nat. Commun.* **11**, 810 (2020).
19. Stetson, L. C. *et al.* Single cell RNA sequencing of AML initiating cells reveals RNA-based evolution during disease progression. *Leukemia* **35**, 2799–2812 (2021).
20. Handsaker, R. E. *et al.* Long somatic DNA-repeat expansion drives neurodegeneration in Huntington's disease. *bioRxiv* (2024) doi:10.1101/2024.05.17.592722.
21. Benson, G. Tandem repeats finder: a program to analyze DNA sequences. *Nucleic Acids Res.* **27**, 573–580 (1999).
22. Mousavi, N., Shleizer-Burko, S., Yanicky, R. & Gymrek, M. Profiling the genome-wide landscape of tandem repeat expansions. *Nucleic Acids Res.* **47**, e90 (2019).
23. Willems, T. *et al.* Genome-wide profiling of heritable and de novo STR variations. *Nat. Methods* **14**, 590–592 (2017).
24. Halman, A., Dolzhenko, E. & Oshlack, A. STRipy: A graphical application for enhanced genotyping of pathogenic short tandem repeats in sequencing data. *Hum. Mutat.* **43**, 859–868 (2022).
25. GitHub - Illumina/RepeatCatalogs. *GitHub* https://github.com/Illumina/RepeatCatalogs.
26. Weisburd, B., Tiao, G. & Rehm, H. L. Insights from a genome-wide truth set of tandem repeat variation. *bioRxiv* (2023) doi:10.1101/2023.05.05.539588.
27. Weisburd, B. *et al.* Defining a tandem repeat catalog and variation clusters for

genome-wide analyses and population databases. *bioRxiv* (2024) doi:10.1101/2024.10.04.615514.

28. Dolzhenko, E. *et al.* Resolving the unsolved: Comprehensive assessment of tandem repeats at scale. *bioRxiv* (2023) doi:10.1101/2023.05.12.540470.
29. Steely, C. J., Watkins, W. S., Baird, L. & Jorde, L. B. The mutational dynamics of short tandem repeats in large, multigenerational families. *Genome Biol.* **23**, 253 (2022).
30. Morales, J. *et al.* A joint NCBI and EMBL-EBI transcript set for clinical genomics and research. *Nature* **604**, 310–315 (2022).
31. Dolzhenko, E. *et al.* ExpansionHunter: a sequence-graph-based tool to analyze variation in short tandem repeat regions. *Bioinformatics* **35**, 4754–4756 (2019).
32. Dolzhenko, E. *et al.* Detection of long repeat expansions from PCR-free whole-genome sequence data. *Genome Res.* **27**, 1895–1903 (2017).
33. Mallick, S. *et al.* The Simons Genome Diversity Project: 300 genomes from 142 diverse populations. *Nature* **538**, 201–206 (2016).
34. Kimura, M. & Ohta, T. Stepwise mutation model and distribution of allelic frequencies in a finite population. *Proc. Natl. Acad. Sci. U. S. A.* **75**, 2868–2872 (1978).
35. Urbut, S. M., Wang, G., Carbonetto, P. & Stephens, M. Flexible statistical methods for estimating and testing effects in genomic studies with multiple conditions. *Nat. Genet.* **51**, 187–195 (2019).
36. Alquicira-Hernandez, J., Sathe, A., Ji, H. P., Nguyen, Q. & Powell, J. E. scPred: accurate supervised method for cell-type classification from single-cell RNA-seq data. *Genome Biol* **20**, 264 (2019).
37. Franco, A. *et al.* CD21 and FCRL5 form a receptor complex with robust B-cell activating capacity. *Int. Immunol.* **30**, 569–578 (2018).
38. Thomas, P. D. *et al.* PANTHER: Making genome-scale phylogenetics accessible to all. *Protein Sci* **31**, 8–22 (2022).
39. Ashburner, M. *et al.* Gene ontology: tool for the unification of biology. The Gene Ontology Consortium. *Nat Genet* **25**, 25–29 (2000).

40. Gene Ontology Consortium *et al.* The Gene Ontology knowledgebase in 2023. *Genetics* **224**, (2023).
41. Natri, H. M. *et al.* Cell-type-specific and disease-associated expression quantitative trait loci in the human lung. *Nat. Genet.* **56**, 595–604 (2024).
42. Mu, Z. *et al.* The impact of cell type and context-dependent regulatory variants on human immune traits. *Genome Biol.* **22**, 122 (2021).
43. Sha, J. *et al.* The B-Cell-Specific Ablation of B4GALT1 Reduces Cancer Formation and Reverses the Changes in Serum IgG Glycans during the Induction of Mouse Hepatocellular Carcinoma. *Cancers* **14**, (2022).
44. Cui, Y. *et al.* B4GALT1 promotes immune escape by regulating the expression of PD-L1 at multiple levels in lung adenocarcinoma. *J. Exp. Clin. Cancer Res.* **42**, 146 (2023).
45. Bakhtiari, M. *et al.* Variable number tandem repeats mediate the expression of proximal genes. *Nat. Commun.* **12**, 2075 (2021).
46. Lek, M. *et al.* Analysis of protein-coding genetic variation in 60,706 humans. *Nature* **536**, 285–291 (2016).
47. Andrews, G. *et al.* Mammalian evolution of human cis-regulatory elements and transcription factor binding sites. *Science* **380**, eabn7930 (2023).
48. Kuderna, L. F. K. *et al.* Identification of constrained sequence elements across 239 primate genomes. *Nature* **625**, 735–742 (2024).
49. Deaton, A. M. & Bird, A. CpG islands and the regulation of transcription. *Genes Dev* **25**, 1010–1022 (2011).
50. Fenouil, R. *et al.* CpG islands and GC content dictate nucleosome depletion in a transcription-independent manner at mammalian promoters. *Genome Res* **22**, 2399–2408 (2012).
51. Taylor, K. H. *et al.* Large-scale CpG methylation analysis identifies novel candidate genes and reveals methylation hotspots in acute lymphoblastic leukemia. *Cancer Res.* **67**, 2617–2625 (2007).
52. Golding, A., Rosen, A., Petri, M., Akhter, E. & Andrade, F. Interferon-alpha regulates the

dynamic balance between human activated regulatory and effector T cells: implications for antiviral and autoimmune responses. *Immunology* **131**, 107–117 (2010).

53. Xu, S. *et al.* Cytosolic phospholipase A2 gamma is involved in hepatitis C virus replication and assembly. *J Virol* **86**, 13025–13037 (2012).
54. Gall-Duncan, T., Sato, N., Yuen, R. K. C. & Pearson, C. E. Advancing genomic technologies and clinical awareness accelerates discovery of disease-associated tandem repeat sequences. *Genome Res.* **32**, 1–27 (2022).
55. Lamkin, M. & Gymrek, M. The emerging role of tandem repeats in complex traits. *Nat Rev Genet* **25**, 452–453 (2024).
56. Martin, A. R. *et al.* PanelApp crowdsources expert knowledge to establish consensus diagnostic gene panels. *Nat. Genet.* **51**, 1560–1565 (2019).
57. Liu, Z. *et al.* Genetic architecture of the inflammatory bowel diseases across East Asian and European ancestries. *Nat. Genet.* **55**, 796–806 (2023).
58. Ishigaki, K. *et al.* Multi-ancestry genome-wide association analyses identify novel genetic mechanisms in rheumatoid arthritis. *Nat. Genet.* **54**, 1640–1651 (2022).
59. Bentham, J. *et al.* Genetic association analyses implicate aberrant regulation of innate and adaptive immunity genes in the pathogenesis of systemic lupus erythematosus. *Nat. Genet.* **47**, 1457–1464 (2015).
60. Michailidou, K. *et al.* Association analysis identifies 65 new breast cancer risk loci. *Nature* **551**, 92–94 (2017).
61. Fernandez-Rozadilla, C. *et al.* Deciphering colorectal cancer genetics through multi-omic analysis of 100,204 cases and 154,587 controls of European and east Asian ancestries. *Nat. Genet.* **55**, 89–99 (2023).
62. McKay, J. D. *et al.* Large-scale association analysis identifies new lung cancer susceptibility loci and heterogeneity in genetic susceptibility across histological subtypes. *Nat. Genet.* **49**, 1126–1132 (2017).
63. Sakaue, S. *et al.* A cross-population atlas of genetic associations for 220 human phenotypes. *Nat. Genet.* **53**, 1415–1424 (2021).

64. Wang, A. *et al.* Characterizing prostate cancer risk through multi-ancestry genome-wide discovery of 187 novel risk variants. *Nat. Genet.* **55**, 2065–2074 (2023).
65. COVID-19 Host Genetics Initiative. The COVID-19 Host Genetics Initiative, a global initiative to elucidate the role of host genetic factors in susceptibility and severity of the SARS-CoV-2 virus pandemic. *Eur. J. Hum. Genet.* **28**, 715–718 (2020).
66. Bellenguez, C. *et al.* New insights into the genetic etiology of Alzheimer's disease and related dementias. *Nat. Genet.* **54**, 412–436 (2022).
67. Nalls, M. A. *et al.* Identification of novel risk loci, causal insights, and heritable risk for Parkinson's disease: a meta-analysis of genome-wide association studies. *Lancet Neurol.* **18**, 1091–1102 (2019).
68. Giambartolomei, C. *et al.* Bayesian test for colocalisation between pairs of genetic association studies using summary statistics. *PLoS Genet.* **10**, e1004383 (2014).
69. Weaver, N. *et al.* KIF16B Mediates Anterograde Transport and Modulates Lysosomal Degradation of the HIV-1 Envelope Glycoprotein. *J. Virol.* **97**, e0025523 (2023).
70. Adam, F. *et al.* Kinesin-1 Is a New Actor Involved in Platelet Secretion and Thrombus Stability. *Arterioscler. Thromb. Vasc. Biol.* **38**, 1037–1051 (2018).
71. Kurowska, M. *et al.* Terminal transport of lytic granules to the immune synapse is mediated by the kinesin-1/Slp3/Rab27a complex. *Blood* **119**, 3879–3889 (2012).
72. Ogbomo, H. *et al.* Granule-Dependent NK Cell Killing of Cryptococcus Requires Kinesin to Reposition the Cytolytic Machinery for Directed Cytotoxicity. *Cell Rep.* **24**, 3017–3032 (2018).
73. Ponomarev, E. D. Fresh Evidence for Platelets as Neuronal and Innate Immune Cells: Their Role in the Activation, Differentiation, and Deactivation of Th1, Th17, and Tregs during Tissue Inflammation. *Front Immunol* **9**, 406 (2018).
74. Tsukamoto, H., Huston, G. E., Dibble, J., Duso, D. K. & Swain, S. L. Bim dictates naive CD4 T cell lifespan and the development of age-associated functional defects. *J. Immunol.* **185**, 4535–4544 (2010).
75. Wojciechowski, S. *et al.* Bim/Bcl-2 balance is critical for maintaining naive and memory

T cell homeostasis. *J. Exp. Med.* **204**, 1665–1675 (2007).

76. Imam, T., Park, S., Kaplan, M. H. & Olson, M. R. Effector T Helper Cell Subsets in Inflammatory Bowel Diseases. *Front. Immunol.* **9**, 1212 (2018).
77. Hahne, F. & Ivanek, R. Visualizing Genomic Data Using Gviz and Bioconductor. *Methods Mol Biol* **1418**, 335–351 (2016).
78. Zhou, Y. *et al.* FAM117B promotes gastric cancer growth and drug resistance by targeting the KEAP1/NRF2 signaling pathway. *J. Clin. Invest.* **133**, (2023).
79. Kamisako, T. *et al.* Role of Nrf2 in the alteration of cholesterol and bile acid metabolism-related gene expression by dietary cholesterol in high fat-fed mice. *J. Clin. Biochem. Nutr.* **54**, 90–94 (2014).
80. Lusis, A. J. Atherosclerosis. *Nature* **407**, 233–241 (2000).
81. Sabbah, N., Jaisson, S., Garnotel, R., Anglés-Cano, E. & Gillery, P. Small size apolipoprotein(a) isoforms enhance inflammatory and proteolytic potential of collagen-primed monocytes. *Lipids Health Dis.* **18**, 166 (2019).
82. Wang, C., Kang, S. G., Lee, J., Sun, Z. & Kim, C. H. The roles of CCR6 in migration of Th17 cells and regulation of effector T-cell balance in the gut. *Mucosal Immunol.* **2**, 173–183 (2009).
83. Suan, D. *et al.* CCR6 Defines Memory B Cell Precursors in Mouse and Human Germinal Centers, Revealing Light-Zone Location and Predominant Low Antigen Affinity. *Immunity* **47**, 1142–1153.e4 (2017).
84. Wang, Y. *et al.* Rheumatoid arthritis patients display B-cell dysregulation already in the naïve repertoire consistent with defects in B-cell tolerance. *Sci. Rep.* **9**, 19995 (2019).
85. Lörchner, H. *et al.* Neutrophils for Revascularization Require Activation of CCR6 and CCL20 by TNFα. *Circ. Res.* **133**, 592–610 (2023).
86. Sarafidou, T., Galliopoulou, E., Apostolopoulou, D., Fragkiadakis, G. A. & Moschonas, N. K. Reconstruction of a Comprehensive Interactome and Experimental Data Analysis of FRA10AC1 May Provide Insights into Its Biological Role in Health and Disease. *Genes (Basel)* **14**, (2023).

87. Al-Mahdawi, S. *et al.* The Friedreich ataxia GAA repeat expansion mutation induces comparable epigenetic changes in human and transgenic mouse brain and heart tissues. *Hum Mol Genet* **17**, 735–746 (2008).

88. Khristich, A. N. & Mirkin, S. M. On the wrong DNA track: Molecular mechanisms of repeat-mediated genome instability. *J Biol Chem* **295**, 4134–4170 (2020).

89. McMurray, C. T. Mechanisms of trinucleotide repeat instability during human development. *Nat Rev Genet* **11**, 786–799 (2010).

90. Niu, Y. *et al.* Multiparametric and accurate functional analysis of genetic sequence variants using CRISPR-Select. *Nat Genet* **54**, 1983–1993 (2022).

91. Dobin, A. *et al.* STAR: ultrafast universal RNA-seq aligner. *Bioinformatics* **29**, 15–21 (2013).

92. Neavin, D. *et al.* Demuxafy: improvement in droplet assignment by integrating multiple single-cell demultiplexing and doublet detection methods. *Genome Biol.* **25**, 94 (2024).

93. str-analysis/str_analysis/variant_catalogs/variant_catalog_without_offtargets.GRCh38.json at main · broadinstitute/str-analysis. *GitHub* https://github.com/broadinstitute/str-analysis/blob/main/str_analysis/variant_catalogs/variant_catalog_without_offtargets.GRCh38.json.

94. Hinrichs, A. S. *et al.* The UCSC Genome Browser Database: update 2006. *Nucleic Acids Res.* **34**, D590–8 (2006).

95. Pemberton, T. J., Sandefur, C. I., Jakobsson, M. & Rosenberg, N. A. Sequence determinants of human microsatellite variability. *BMC Genomics* **10**, 612 (2009).

96. Willems, T. *et al.* The landscape of human STR variation. *Genome Res.* **24**, 1894–1904 (2014).

97. Mousavi, N. *et al.* TRTools: a toolkit for genome-wide analysis of tandem repeats. *Bioinformatics* **37**, 731–733 (2021).

98. Bais, A. S. & Kostka, D. scds: computational annotation of doublets in single-cell RNA sequencing data. *Bioinformatics* **36**, 1150–1158 (2020).

99. Huang, Y., McCarthy, D. J. & Stegle, O. Vireo: Bayesian demultiplexing of pooled single-cell RNA-seq data without genotype reference. *Genome Biol* **20**, 273 (2019).

100. Germain, P.-L., Lun, A., Garcia Meixide, C., Macnair, W. & Robinson, M. D. Doublet identification in single-cell sequencing data using. *F1000Res* **10**, 979 (2021).

101. Wolf, F. A., Angerer, P. & Theis, F. J. SCANPY: large-scale single-cell gene expression data analysis. *Genome Biol* **19**, 15 (2018).

102. Cuomo, A. S. E. *et al.* Optimizing expression quantitative trait locus mapping workflows for single-cell studies. *Genome Biol.* **22**, 188 (2021).

103. Balduzzi, S., Rücker, G. & Schwarzer, G. How to perform a meta-analysis with R: a practical tutorial. *Evid Based Ment Health* **22**, 153–160 (2019).

104. Liu, Y. *et al.* ACAT: A Fast and Powerful p Value Combination Method for Rare-Variant Analysis in Sequencing Studies. *Am. J. Hum. Genet.* **104**, 410–421 (2019).

105. Storey, J. D. The positive false discovery rate: a Bayesian interpretation and the q-value. *Ann. Stat.* **31**, 2013–2035 (2003).

106. Zou, Y., Carbonetto, P., Wang, G. & Stephens, M. Fine-mapping from summary data with the ‘Sum of Single Effects’ model. *PLoS Genet.* **18**, e1010299 (2022).